Accelerated hydrological cycle over the Sanjiangyuan region induces more streamflow extremes at different global warming levels

Peng Ji[1,2], Xing Yuan[3], Feng Ma[3], Ming Pan[4]

[1]Key Laboratory of Regional Climate-Environment for Temperate East Asia, Institute of Atmospheric Physics, Chinese Academy of Sciences, Beijing 100029, China

[2]College of Earth and Planetary Sciences, University of Chinese Academy of Sciences, Beijing 1000493, China

[3]School of Hydrology and Water Resources, Nanjing University of Information Science and Technology, Nanjing 210044, China

[4]Department of Civil and Environmental Engineering, Princeton University, Princeton, New Jersey, USA

Correspondence to: Xing Yuan (xyuan@nuist.edu.cn)

16 **Abstract.** Serving source water for the Yellow, Yangtze and Lancang-Mekong rivers,

17 the Sanjiangyuan region concerns 700 million people over its downstream areas.

18 Recent research suggests that the Sanjiangyuan region will become wetter in a

19 warming future, but future changes in streamflow extremes remain unclear due to the

20 complex hydrological processes over high-land areas and limited knowledge of the

21 influences of land cover change and CO_2 physiological forcing. Based on high

22 resolution land surface modeling during 1979~2100 driven by the climate and

23 ecological projections from 11 newly released Coupled Model Intercomparison

24 Project Phase 6 (CMIP6) climate models, we show that different accelerating rates of

25 precipitation and evapotranspiration at 1.5 ℃ global warming level induce 55% more

26 dry extremes over Yellow river and 138% more wet extremes over Yangtze river

27 headwaters compared with the reference period (1985~2014). An additional 0.5 ℃

28 warming leads to a further nonlinear and more significant increase for both dry

29 extremes over Yellow river (22%) and wet extremes over Yangtze river (64%). The

30 combined role of CO_2 physiological forcing and vegetation greening, which used to

31 be neglected in hydrological projections, is found to alleviate dry extremes at 1.5 and

32 2.0 ℃ warming levels but to intensify dry extremes at 3.0 ℃ warming level. Moreover,

33 vegetation greening contributes half of the differences between 1.5 and 3.0 ℃

34 warming levels. This study emphasizes the importance of ecological processes in

35 determining future changes in streamflow extremes, and suggests a "dry gets drier,

36 wet gets wetter" condition over headwaters.

37 **Keywords** Terrestrial hydrological cycle, streamflow extremes, global warming levels,

38 CMIP6, Sanjiangyuan, land cover change

1 Introduction

Global temperature has increased at a rate of 1.7 °C/decade since 1970, contrary to the cooling trend over the past 8000 years (Marcott et al., 2013). The temperature measurements suggest that 2015-2019 is the warmest five years and 2010-2019 is also the warmest decade since 1850 (WMO, 2020). To mitigate the impact of this unprecedented warming on the global environment and human society, 195 nations adopted the Paris Agreement which decides to "hold the increase in the global average temperature to well below 2 °C above pre-industrial levels and pursing efforts to limit the temperature increase to 1.5 °C".

The response of regional and global terrestrial hydrological processes, including streamflow and its extremes, to different global warming levels has been investigated by numerous studies in recent years (Chen et al., 2017; Döll et al., 2018; Marx et al., 2018; Mohammed et al., 2017; Thober et al., 2018; Zhang et al., 2016). In addition to climate change, recent works reveal the importance of the ecological factors (e.g., the CO_2 physiological forcing and land cover change), which are often unaccounted for in hydrological modeling works, in modulating the streamflow and its extremes. For example, the increasing CO_2 concentration is found to alleviate the decreasing trend of streamflow in the future at global scale, because the increased CO_2 concentration will decrease the vegetation transpiration by reducing the stomatal conductance (known as the CO_2 physiological forcing) (Fowler et al., 2019; Wiltshire et al., 2013; Yang et al., 2019; Zhu et al., 2012). Contrary to the CO_2 physiological forcing, the vegetation greening in a warming climate is found to have a significant role on

61   exacerbating hydrological drought, as it enhances transpiration and dries up the land

62   (Yuan et al., 2018b). However, the relative importance of CO_2 physiological forcing

63   and vegetation greening in influencing the terrestrial hydrology especially the

64   streamflow extremes is still unknown, and whether their combined impact changes at

65   different warming levels remains to be investigated.

66   Hosting the headwaters of the Yellow river, the Yangtze river and the

67   Lancang-Mekong river, the Sanjiangyuan region is known as the "Asian Water

68   Tower" and concerns 700 million people over its downstream. Changes of streamflow

69   and streamflow extremes over the Sanjiangyuan not only influence the local

70   ecosystem and water resource, but also affect the security of food, energy, and water

71   over the downstream areas. Both the regional climate and ecosystem show significant

72   changes over the Sanjiangyuan due to global warming (Bibi et al., 2018; Kuang and

73   Jiao, 2016; Liang et al., 2013; Yang et al., 2013; Zhu et al., 2016), which makes the

74   Sanjiangyuan a representative region to investigate the role of climate change and

75   ecological change (e.g., land use change and CO_2 physiological forcing) in

76   influencing the streamflow and its extremes (Cuo et al., 2014; Ji and Yuan, 2018; Zhu

77   et al., 2013). For example, historical changes in climate and ecology (e.g. land cover)

78   are found to cause significant reduction in mean and high flows during 1979-2005,

79   which potentially increases drought risk over its downstream areas (Ji and Yuan,

80   2018). And the CO_2 physiological forcing is revealed to cause equally large changes

81   in regional flood extremes as the precipitation over the Yangtze and Mekong rivers

82   (Fowler et al., 2019). Recent research suggests that the Sanjiangyuan region will

83 become warmer and wetter in the future, and extreme precipitation will also increase

84 at the 1.5℃ global warming level and further intensify with a 0.5℃ additional

85 warming (Li et al., 2018; Zhao et al., 2019). However, how the streamflow extremes

86 would respond to the 1.5℃ warming, what an additional 0.5℃ or even greater

87 warming would cause, and how much contributions do the ecological factors (e.g.,

88 CO_2 physiological forcing and land cover change) have, are still unknown. This

89 makes it difficult to assess the climate and ecological impact on this vital headwaters

90 region.

91 In this study, we investigate the future changes in the streamflow extremes over

92 the Sanjiangyuan region from an integrated eco-hydrological perspective by taking

93 CO_2 physiological forcing and land cover change into consideration. The combined

94 impacts of the above two ecological factors at different global warming levels are also

95 quantified and compared with the impact of climate change. The results will help

96 understand the role of ecological factors in future terrestrial hydrological changes

97 over the headwater regions like the Sanjiangyuan, and provide guidance and support

98 for the stakeholders to make relevant decisions and plans.

99 **2 Data and methods**

100 **2.1 Study domain and observational data**

101 The Sanjiangyuan region is located at the eastern part of the Tibetan Plateau

102 (Figure 1a), with the total area and mean elevation being 3.61×10^5 km^2 and 5000 m

103 respectively. It plays a critical role in providing fresh water, by contributing 35, 20

104 and 8% to the total annual streamflow of the Yellow, Yangtze and Lancang-Mekong

105 rivers (Li et al., 2017; Liang et al., 2013). The source regions of Yellow, Yangtze and

106 Lancang-Mekong rivers account for 46, 44 and 10% of the total area of the

107 Sanjiangyuan individually, and the Yellow river source region has a warmer climate

108 and sparer snow cover than the Yangtze river source region.

109   Monthly streamflow observations from the Tangnaihai (TNH) and the Zhimenda

110 (ZMD) hydrological stations (Figure 1a), which were provided by the local authorities,

111 were used to evaluate the streamflow simulations. Data periods are 1979-2011 and

112 1980-2008 for the Tangnaihai and Zhimenda stations individually. Monthly terrestrial

113 water storage change observation and its uncertainty during 2003-2014 was provided

114 by the Jet Propulsion Laboratory (JPL), which used the mass concentration blocks

115 (mascons) basis functions to fit the Gravity Recovery and Climate Experiment

116 (GRACE) satellite's inter-satellite ranging observations (Watkins et al., 2015). The

117 Model Tree Ensemble evapotranspiration (MTE_ET; Jung et al., 2009) and the Global

118 Land Evaporation Amsterdam Model evapotranspiration (GLEAM_ET) version 3.3a

119 (Martens et al., 2017) were also used to evaluate the model performance on ET

120 simulation.

121 **2.2 CMIP6 Data**

122   Here, 19 Coupled Model Intercomparison Project phase 6 (CMIP6, Eyring et al.,

123 2016) models which provide precipitation, near-surface temperature, specific

124 humidity, 10-m wind speed, surface downward shortwave and longwave radiations at

125 daily timescale were first selected for evaluation. Then, models were chosen for the

126 analysis when the simulated meteorological forcings (e.g., precipitation, temperature,

127   humidity, and shortwave radiation) averaged over the Sanjiangyuan region have the

128   same trend sign as the observation during 1979-2014. Table 1 shows the 11 CMIP6

129   models that were finally chosen in this study. For the future projection (2015-2100),

130   we chose two Shared Socioeconomic Pathways (SSP) experiments: SSP585 and

131   SSP245. SSP585 combines the fossil-fueled development socioeconomic pathway

132   and $8.5 W/m^2$ forcing pathway (RCP8.5), while SSP245 combines the moderate

133   development socioeconomic pathway and $4.5 W/m^2$ forcing pathway (RCP4.5)

134   (O'Neill et al., 2016). Land cover change is quantified by leaf area index (LAI) as

135   there is no significant transition between different vegetation types (not shown)

136   according   to   the   Land-use   Harmonization   2   (LUH2)   dataset

137   (https://esgf-node.llnl.gov/search/input4mips/). For the CNRM-CM6-1, FGOALS-g3

138   and CESM2, the ensemble mean of LAI simulations from the other 8 CMIP6 models

139   was used because CNRM-CM6-1 and FGOALS-g3 do not provide dynamic LAI

140   while the CESM2 simulates an abnormally large LAI over the Sanjiangyuan region.

141   To avoid systematic bias in meteorological forcing, the trend-preserved bias

142   correction method suggested by ISI-MIP (Hempel et al., 2013), was applied to the

143   CMIP6 model simulations at monthly scale. The China Meteorological Forcing

144   Dataset (CMFD; He et al., 2020) is taken as meteorological observation. For each

145   month, temperature bias in CMIP6 simulations during 1979-2014 was directly

146   deducted. Future temperature simulations in SSP245 and SSP585 experiments were

147   also adjusted according to the historical bias. Other variables were corrected by using

148   a multiplicative factor, which was calculated by using observations to divide

149   simulation during 1979-2014. In addition, monthly leaf area index was also adjusted

150   to be consistent with satellite observation using the same method as temperature. All

151   variables were first interpolated to the 10 km resolution over the Sanjiangyuan region

152   and the bias correction was performed for each CMIP6 model at each grid. After bias

153   correction, absolute changes of temperature and leaf area index, and relative changes

154   of other variables were preserved at monthly time scale (Hempel et al., 2013). Then,

155   the adjusted CMIP6 daily meteorological forcings were disaggregated into hourly

156   using the diurnal cycle ratios from the China Meteorological Forcing Dataset.

157   The historical CO_2 concentration used here is the same as the CMIP6 historical

158   experiment (Meinshausen et al., 2017), while future CO_2 concentration in SSP245 and

159   SSP585 scenarios came from simulations of a reduced-complexity carbon-cycle

160   model MAGICC7.0 (Meinshausen et al., 2020).

161   **2.3 Experimental design**

162   The land surface model used in this study is the Conjunctive Surface-Subsurface

163   Process model version 2 (CSSPv2), which has been proved to simulate the energy and

164   water processes over the Sanjiangyuan region well (Yuan et al., 2018a). Figure 2

165   shows the structure and main ecohydrological processes in CSSPv2. The CSSPv2 is

166   rooted in the Common Land Model (CoLM; Dai et al., 2003) with some

167   improvements at hydrological processes. CSSPv2 has a volume-averaged soil

168   moisture transport (VAST) model, which solves the quasi-three dimensional

169   transportation of the soil water and explicitly considers the variability of moisture flux

170   due to subgrid topographic variations (Choi et al., 2007). Moreover, the Variable

171   Infiltration Capacity runoff scheme (VIC; Liang et al., 1994), and the influences of

172   soil organic matters on soil hydrological properties are incorporated into the CSSPv2

173   by Yuan et al. (2018a), to improve its performance in simulating the terrestrial

174   hydrology over the Sanjiangyuan region. Similar to the CoLM and the Community

175   Land Surface Model (CLM; Oleson et al., 2013), vegetation transpiration in CSSPv2

176   is based on Monin-Obukhov similarity theory, and the transpiration rate is constrained

177   by leaf boundary layer and stomatal conductances. Parameterization of the stomatal

178   conductance (g_s) in CSSPv2 is

179
$$g_s = m \frac{A_n}{P_{CO_2}/P_{atm}} h_s + b\beta_t$$

180   where the m is a plant functional type dependent parameter, A_n is leaf net

181   photosynthesis ($\mu\,mol\,CO_2\,m^{-2}\,s^{-1}$), P_{CO_2} is the CO_2 partial pressure at the leaf

182   surface (Pa), P_{atm} is the atmospheric pressure (Pa), h_s is the lead surface

183   humidity, b is the minimum stomatal conductance ($\mu\,mol\,m^{-2}\,s^{-1}$), while β_t is the

184   soil water stress function. Generally, the stomatal conductance decreases with the

185   increasing of CO_2 concentration.

186   First, bias-corrected meteorological forcings from CMIP6 historical experiment

187   were used to drive the CSSPv2 model (CMIP6_His/CSSPv2). All simulations were

188   conducted for two cycles during 1979-2014 at half-hourly time step and 10 km spatial

189   resolution, with the first cycle serving as the spin-up. Correlation coefficient (CC) and

190   root mean squared error (RMSE) were calculated for the observed and simulated

191   monthly streamflow, annual evapotranspiration and monthly terrestrial water storage,

192   to evaluate the model performance. The King-Gupta efficiency (KGE; Gupta et al.,

193   2009), which is widely used in streamflow evaluations, was also calculated for

194   streamflow simulations. Above metrics were calculated as follows:

$$CC = \frac{\sum_{i=1}^{n}(x_i - \bar{x})(y_i - \bar{y})}{\sqrt{\sum_{i=1}^{n}(x_i - \bar{x})^2 \sum_{i=1}^{n}(y_i - \bar{y})^2}}$$

195

$$RMSE = \sqrt{\frac{\sum_{i=1}^{n}(x_i - y_i)^2}{n}}$$

196

$$KGE = 1 - \sqrt{(1-CC)^2 + (1-\frac{\sigma_x}{\sigma_y})^2 + (1-\frac{\bar{x}}{\bar{y}})^2}$$

197

198   where x_i and y_i are observed and simulated variables in a specific month/year i

199   individually, and $\bar{x}$ and $\bar{y}$ are corresponding monthly/annual means during the

200   whole evaluation period n. The σ_x and σ_y are observed and simulated standard

201   deviations respectively. The correlation coefficient represents the correlation between

202   simulation and observation, while RMSE means simulated error. The KGE ranges

203   from negative infinity to 1 and model simulations can be regard as satisfactory when

204   the KGE is larger than 0.5 (Moriasi et al., 2007).

205   Second, bias-corrected meteorological forcings in SSP245 and SSP585 were

206   used to drive CSSPv2 during 2015-2100 with dynamic LAI and CO_2 concentration

207   (CMIP6_SSP/CSSPv2). Initial conditions of CMIP6_SSP/CSSPv2 came from the last

208   year in CMIP6_His/CSSPv2.

209   Then, the second step was repeated twice by fixing the monthly LAI

210   (CMIP6_SSP/CSSPv2_FixLAI)   and   mean CO_2 concentration

211   (CMIP6_SSP/CSSPv2_FixCO2)   at   2014   level.   The   difference   between

212   CMIP6_SSP/CSSPv2 and CMIP6_SSP/CSSPv2_FixLAI is regarded as the net effect

213   of land cover change, and the difference between CMIP6_SSP/CSSPv2 and

214   CMIP6_SSP/CSSPv2_FixCO2 is regarded as the net effect of CO_2 physiological

215   forcing.

2.4 Warming level determination

217   A widely used time-sampling method was adopted to determine the periods of

218   different global warming levels (Chen et al., 2017; Döll et al., 2018; Marx et al., 2018;

219   Mohammed et al., 2017; Thober et al., 2018). According to the HadCRUT4 dataset

220   (Morice et al., 2012), the global mean surface temperature has increased by 0.66 ℃

221   from the pre-industrial era (1850-1900) to the reference period defined as 1985-2014.

222   Then, starting from 2015, 30-years running mean global temperatures were compared

223   to those of the 1985-2014 period for each GCM simulation. And the

224   1.5 ℃/2.0 ℃/3.0 ℃ warming period is defined as the 30-years period when the

225   0.84 ℃/1.34 ℃/2.34 ℃ global warming, compared with the reference period

226   (1985-2014), is first reached. The median years of identified 30-year periods, referred

227   as "crossing years", are shown in Table 2.

2.5 Definition of dry and wet extremes and robustness assessment

229   In this research, the standardized streamflow index (SSI) was used to define dry

230   and wet extremes (Vicente-Serrano et al., 2012; Yuan et al., 2017). A gamma

231   distribution was first fitted using July-September (flood season) mean streamflow

232   during the reference period. Then the fitted distribution was used to calculate the

233   standardized deviation of the July-September mean streamflow (i.e. SSI) in each year

234   during both the reference and projection periods. Here, dry and wet extremes were

235   defined as where SSIs are smaller than -1.28 (a probability of 10%) and larger than

236   1.28 respectively.

237   The relative changes of dry/wet extremes frequencies between the reference

238   period and different warming periods were first calculated for each GCMs under each

239   SSP scenarios, and the ensemble means were then determined for each warming

240   levels. To quantify the uncertainty, above calculations were repeated by doing

241   bootstrapping 10,000 times, and 11 GCMs were resampled with replacement during

242   each bootstrap (Christopher et al., 2018). The 5% and 95% percentiles of the total

243   10,000 estimations were finally taken as the 5~95% uncertainty ranges.

244   **3 Results**

245   **3.1 Terrestrial hydrological changes at different warming levels**

246   As shown in Figures 1b-1e, observations (pink lines) show that the annual

247   temperature, precipitation and growing season LAI increase at the rates of

248   0.63 ℃/decade (p=0), 16.9 mm/decade (p=0.02), and 0.02 m^2/m^2/decade (p=0.001)

249   during 1979-2014 respectively. The ensemble means of CMIP6 simulations (black

250   lines) can generally capture the historical increasing trends of temperature

251   (0.30 ℃/decade, p=0), precipitation (7.1 mm/decade, p=0) and growing season LAI

252   (0.029 m^2/m^2/decade, p=0), although the increasing trends of precipitation and

253   temperature are underestimated. In 2015-2100, the SSP245 scenario (blue lines)

254   shows continued warming, wetting and greening trends, and the trends are larger in

255   the SSP585 scenario (red lines). The CO_2 concentration also keeps increasing during

256 2015-2100 and reaches to 600 ppm and 1150 ppm in 2100 for the SSP245 and

257 SSP585 scenarios respectively. Although the SSP585 scenario reaches the same

258 warming levels earlier than the SSP245 scenario (Table 2), there is no significant

259 difference between them in the meteorological variables during the same warming

260 period (not shown). Thus, we do not distinguish SSP245 and SSP585 scenarios at the

261 same warming level in the following analysis.

262   Figure 3 and Table 3 show the evaluation of model simulation. Driven by

263 observed meteorological and ecological forcings, the CMFD/CSSPv2 simulates

264 monthly streamflow over the Yellow and Yangtze river headwaters quite well.

265 Compared with the observation at Tangnaihai (TNH) and Zhimenda (ZMD) stations,

266 the Kling-Gupta efficiencies of the CMFD/CSSPv2 simulated monthly streamflow are

267 0.94 and 0.91 respectively. The simulated monthly Terrestrial Water Storage Anomaly

268 (TWSA) during 2003-2014 in CMFD/CSSPv2 also agrees with the GRACE satellite

269 observation and captures the increasing trend. For the interannual variations of

270 evapotranspiration, CMFD/CSSPv2 is consistent with the ensemble mean of the

271 GLEAM_ET and MTE_ET products, and the correlation coefficient and root mean

272 squared error (RMSE) during 1982-2011 are 0.87 (p<0.01) and 14 mm/year

273 respectively. This suggests the good performance of the CSSPv2 in simulating the

274 hydrological processes over the Sanjiangyuan region. Although meteorological and

275 ecological outputs from CMIP6 models have coarse resolutions (~100km), the land

276 surface simulation driven by bias corrected CMIP6 results (CMIP6_His/CSSPv2) also

277 captures the terrestrial hydrological variations reasonably well. The Kling-Gupta

278   efficiency of the ensemble mean streamflow simulation reaches up to 0.71~0.81, and

279   the ensemble mean monthly Terrestrial Water Storage Anomaly (TWSA) and annual

280   evapotranspiration generally agree with observations and other reference data

281   (Figures 3c-d).

282   Figure 4 shows relative changes of terrestrial hydrological variables over the

283   Sanjiangyuan region at different warming levels. The ensemble mean of the increase

284   in annual precipitation is 5% at 1.5 ℃ warming level, and additional 0.5 ℃ and 1.5 ℃

285   warming will further increase the wetting trends to 7% and 13% respectively. Annual

286   evapotranspiration experiences significant increases at all warming levels, and the

287   ensemble mean increases are 4%, 7% and 13% at 1.5, 2.0 and 3.0 ℃ warming levels

288   respectively. The ratio of transpiration to evapotranspiration also increases

289   significantly, indicating that vegetation transpiration increases much larger than the

290   soil evaporation and canopy evaporation. Although annual total runoff has larger

291   relative changes than evapotranspiration (6%, 9% and 14% at 1.5, 2.0 and 3.0 ℃

292   warming levels respectively), the uncertainty is large as only 75% of the models show

293   positive signals, which may be caused by large uncertainty in the changes during

294   summer and autumn seasons. The terrestrial water storage (TWS) which includes

295   foliage water, surface water, soil moisture and groundwater, shows slightly decreasing

296   trend at annual scale, suggesting that the increasing precipitation in the future

297   becomes extra evapotranspiration and runoff instead of recharging the local water

298   storage. The accelerated terrestrial hydrological cycle also exists at seasonal scale, as

299   the seasonal changes are consistent with the annual ones.

3.2 Changes in streamflow extremes at different warming levels

Although the intensified terrestrial hydrology induces more streamflow over the headwater region of Yellow river during winter and spring months, streamflow does not increase and even decreases during the flood season (July-September; Figure 5a). Figure 5b shows the changes of streamflow dry extremes over the Yellow river source region at different warming levels, with the error bars showing estimated uncertainties. The frequency of streamflow dry extremes over the Yellow river is found to increase by 55% at 1.5 ℃ warming level (Figure 5b), but the uncertainty is larger than the ensemble mean. However, the dry extreme frequency will further increase to 77% and 125% at the 2.0 and 3.0 ℃ warming levels and the results become significant (Figure 5b). No significant changes are found for the wet extremes at all warming levels over the Yellow River headwater region, as the uncertainty ranges are lager than the ensemble means.

Over the Yangtze river headwater region, streamflow increases in all months at different warming levels (Figure 5c). The frequency of wet extremes increases significantly by 138%, 202% and 232% at 1.5, 2.0 and 3.0 ℃ warming levels (Figure 4d), suggesting a higher risk of flooding. Although the frequency of dry extremes tends to decrease significantly by 35%, 44%, 34% at the three warming levels, the changes are much smaller than those of the wet extremes. Moreover, contributions from climate change and ecological change are both larger than the uncertainty ranges (not shown), suggesting that their impacts on the changes of dry extremes over the Yangtze river headwater region are not distinguishable. Thus, we mainly focus on the

322 dry extremes over the Yellow river and the wet extremes over the Yangtze river in the

323 following analysis.

324   Different changes of streamflow extremes over the Yellow and Yangtze rivers

325 can be interpreted from different accelerating rates of precipitation and

326 evapotranspiration. Figure 6 shows probability density functions (PDFs) of

327 precipitation, evapotranspiration and their difference (P-ET, i.e. residual water for

328 runoff generation) during the flood season. Over the Yellow river, PDFs of

329 precipitation and evapotranspiration both shift to the right against the reference period,

330 except for the precipitation at 1.5 ℃ warming level. However, the increasing trend of

331 evapotranspiration is stronger than that of precipitation, leading to a left shift of PDF

332 for P-ET. Moreover, increased variations of precipitation and evapotranspiration, as

333 indicated by the increased spread of their PDFs, also lead to a larger spread of PDFs

334 of P-ET. The above two factors together induce a heavier left tail in the PDF of P-ET

335 for the warming future than the reference period (Figure 6e). The probability of

336 P-ET<80mm increases from 0.1 during historical period to 0.11, 0.13 and 0.16 at 1.5,

337 2.0 and 3.0 ℃ warming levels individually. This indicates a higher probability of less

338 water left for runoff generation at different warming levels, given little changes in

339 TWS (section 3.1). Moreover, Figure 6e also shows little change to the right tails in

340 the PDF of P-ET as probability for P-ET>130mm stays around 0.1 at different

341 warming levels, suggesting little change to the probability of high residual water. This

342 is consistent with the insignificant wet extreme change over the Yellow river. Over the

343 Yangtze river, however, intensified precipitation is much larger than the increased

344 evapotranspiration, leading to a systematic rightward shift of the PDF of P-ET

345 (Figures 6b, 6d and 6f). Thus both the dry and wet extremes show significant changes

346 over the Yangtze river.

347 **3.3 Influences of land cover change and CO_2 physiological forcing**

348   Figures 7a-7b show the changes of streamflow extremes (compared with the

349 reference period) induced by climate and ecological factors. Although the contribution

350 from climate change (red bars in Figures. 7a-7b) is greater than the ecological factors

351 (blue and cyan bars in in Figures. 7a-7b), influences of CO_2 physiological forcing and

352 land cover change are nontrivial. The CO_2 physiological forcing tends to alleviate dry

353 extremes (or increase wet extremes), while land cover change plays a contrary role.

354 Over the Yellow river, the combined impact of the two ecological factors (sum of blue

355 and cyan bars) reduces the increasing trend of dry extremes caused by climate change

356 (red bars) by 18~22% at 1.5 and 2.0 ℃ warming levels, while intensifies the dry

357 extremes by 9% at 3.0 ℃ warming level. This can be interpreted from their

358 contributions to the evapotranspiration, as the increased LAI enhancement on ET is

359 weaker than the suppression effect of CO_2 physiological impact at 1.5 and 2.0 ℃

360 warming levels, while stronger at 3.0 ℃ warming level (not shown). Over the Yangtze

361 river, similarly, combined effect of land cover and CO_2 physiological forcing

362 increases the wet extremes by 9% at 1.5 ℃ warming level while decreases the wet

363 extremes by 12% at 3.0 ℃ warming level.

364   In addition, Figures 7c and 7d show that the combined impact of CO_2

365 physiological forcing and land cover change also influences the differences between

366 different warming levels. Over the Yellow river, climate change increases dry

367 extremes by 26% from 1.5 to 2.0 ℃ warming level, and by 40% from 1.5 and 3.0 ℃

368 warming level (red bars in Figure 7c). After considering the two ecological factors

369 (pink bars in Figure 7c), above two values change to 22% and 70% respectively, and

370 the difference between 1.5 and 3.0 ℃ warming levels becomes significant. For the wet

371 extreme over the Yangtze river (Figure 7d), the climate change induced difference

372 between 1.5 and 2.0 ℃ warming levels is decreased by 16% after accounting for the

373 two ecological factors. And this decrease reaches up to 49% for the difference

374 between 1.5 and 3.0 ℃ warming levels. We also compared the scenarios when CO_2

375 physiological forcing and land cover change are combined with climate change

376 individually (blue and cyan bars in Figures 7c-d), and the results show the land cover

377 change dominates their combined influences on the difference between different

378 warming levels.

379 **4 Conclusions and Discussion**

380 This study investigates changes of streamflow extremes over the Sanjiangyuan

381 region at different global warming levels through high-resolution land surface

382 modeling driven by CMIP6 climate simulations. The terrestrial hydrological cycle

383 under global warming of 1.5 ℃ is found to accelerate by 4~6% compared with the

384 reference period of 1985-2014, according to the relative changes of precipitation,

385 evapotranspiration and total runoff. The terrestrial water storage, however, shows

386 slight but significant decreasing trend as increased evapotranspiration and runoff are

387 larger than the increased precipitation. This decreasing trend of terrestrial water

storage in the warming future is also found in six major basins in China (Jia et al., 2020). Although streamflow changes during the flood season has a large uncertainty, the frequency of wet extremes over the Yangtze river will increase significantly by 138% and that of dry extremes over the Yellow river will increase by 55% compared with that during 1985~2014. With an additional 0.5℃ warming, the frequency of dry and wet extremes will increase further by 22~64%. If the global warming is not adequately managed (e.g., to reach 3.0℃), wet extremes over the Yangtze river and dry extremes over the Yellow river will increase by 232% and 125%. The changes from 1.5 to 2.0 and 3.0℃ are nonlinear compared with that from reference period to 1.5℃, which are also found for some fixed-threshold climate indices over the Europe (Dosio and Fischer, 2018). It is necessary to cap the global warming at 2℃ or even lower level, to reduce the risk of wet and dry extremes over the Yangtze and Yellow rivers.

This study also shows the nontrivial contributions from land cover change and CO_2 physiological forcing to the extreme streamflow changes especially at 2.0 and 3.0℃ warming levels. The CO_2 physiological forcing is found to increase streamflow and reduce the dry extreme frequency by 14~24%, which is consistent with previous research that CO_2 physiological forcing would increase available water and reduce water stress at the end of this century (Wiltshire et al., 2013). However, our results further show that the drying effect of increasing LAI on streamflow will exceed the wetting effect of CO_2 physiological forcing at 3.0℃ warming level (during 2048~2075) over the Sanjiangyuan region, making a reversion in the combined

410   impacts of CO_2 physiological forcing and land cover. Thus it is vital to consider the

411   impact of land cover change in the projection of future water stress especially at high

412   warming scenarios.

413   Moreover, about 43~52% of the extreme streamflow changes between 1.5 and

414   3.0 ℃ warming levels are attributed to the increased LAI. Considering the LAI

415   projections from different CMIP6 models are induced by the climate change, it can be

416   inferred that the indirect influence of climate change (e.g., through land cover change)

417   has the same and even larger importance on the changes of streamflow extremes

418   between 1.5 and 3.0 ℃ or even higher warming levels, compared with the direct

419   influence (e.g., through precipitation and evapotranspiration). Thus, it is vital to

420   investigate hydrological and its extremes changes among different warming levels

421   from an eco-hydrological perspective instead of focusing on climate change alone.

422   Although we used 11 CMIP6 models combined with two SSP scenarios to reduce

423   the uncertainty of future projections caused by GCMs, using a single land surface

424   model may lead to some uncertainties (Marx et al., 2018). However, considering the

425   high performance of the CSSPv2 land surface model over the Sanjiangyuan region

426   and the dominate role of GCMs' uncertainty over this region (Zhao et al., 2019;

427   Samaniego et al., 2017), uncertainty from the CSSPv2 model should not influence the

428   robust of the result.

429

430   **Acknowledgments** We thank the World Climate Research Programme's Working

431   Group on Couple modelling for providing CMIP6 data (https://esgf-node.llnl.gov).

432 This work was supported by National Key R&D Program of China

433 (2018YFA0606002) and National Natural Science Foundation of China (41875105,

434 91547103), and the Startup Foundation for Introducing Talent of NUIST.

435

436 **Competing interests**

437 The authors declare that they have no conflict of interest.

438

References

Bibi, S., Wang, L., Li, X., Zhou, J., Chen, D., and Yao, T.: Climatic and associated cryospheric, biospheric, and hydrological changes on the Tibetan Plateau: a review, Int. J. Climatol., 38, e1-e17, https://doi.org/10.1002/joc.5411, 2018.

Chen, J., Gao, C., Zeng, X., Xiong, M., Wang, Y., Jing, C. Krysanova, V., Huang, J., Zhao, N., and Su, B.: Assessing changes of river discharge under global warming of 1.5°C and 2°C in the upper reaches of the Yangtze River Basin: Approach by using multiple-GCMs and hydrological models, Quatern. Int., 453, 1–11, http://dx.doi.org/10.1016/j.quaint.2017.01.017, 2017.

Cuo, L., Zhang, Y., Zhu, F., and Liang, L.: Characteristics and changes of streamflow on the Tibetan Plateau: A review, J. Hydrol.-Reg. Stud., 2, 49–68, https://doi.org/10.1016/j.ejrh.2014.08.004, 2014.

Dai, Y. J., Zeng, X. B., Dickinson, R. E., Baker, I., Bonan, G. B., Bosilovich, M. G., Denning, A. S., Dirmeyer, P. A., Houser, P. R., Niu, G. Y., Oleson, K. W., Schlosser, C. A., and Yang, Z. L.: The Common Land Model. B. Am. Meteorol. Soc., 84, 1013–1024, https://doi.org/10.1175/BAMS-84-8-1013, 2003.

Döll, P., Trautmann, T., Gerten, D., Schmied, H. M., Ostberg, S., Saaed, F., and Schleussner, C.: Risks for the global freshwater system at 1.5°C and 2°C global warming. Environ. Res. Lett., 13, 044038, https://doi.org/10.1088/1748-9326/aab792, 2018.

Dosio, A., and Fischer, E. M.: Will half a degree make a difference? Robust projections of indices of mean and extreme climate in Europe under 1.5°C, 2°

461   C, and 3 ° C global warming, Geophys. Res. Lett., 45.

462   https://doi.org/10.1002/2017GL076222, 2018.

463   Eyring, V., Bony, S., Meehl, G. A., Senior, C. A., Stevens, B., Stouffer, R. J., and

464   Taylor, K. E.: Overview of the Coupled Model Intercomparison Project Phase 6

465   (CMIP6) experimental design and organization, Geosci. Model Dev., 9, 1937–

466   1958. https://doi.org/10.5194/gmd-9-1937-2016, 2016.

467   Fowler, M. D., Kooperman G. J., Randerson, J. T. and Pritchard M. S.: The effect of

468   plant physiological responses to rising CO_2 on global streamflow, Nat. Clim.

469   Change, 9, 873-879, https://doi.org/10.1038/s41558-019-0602-x, 2019.

470   He, J., Yang, K., Tang, W., Lu, H., Qin, J., Chen, Y., and Li, X.: The first

471   high-resolution meteorological forcing dataset for land process studies over

472   China, Sci. Data, 7, 25. https://doi.org/10.1038/s41597-020-0369-y, 2020.

473   Hempel, S., Frieler, K., Warszawski, L., and Piontek, F.: A trend-preserving bias

474   correction-the ISI-MIP approach, Earth Syst. Dyn., 4, 219-236.

475   https://doi.org/10.5194/esd-4-219-2013, 2013.

476   Ji, P., and Yuan, X.: High-resolution land surface modeling of hydrological changes

477   over the Sanjiangyuan region in the eastern Tibetan Plateau: 2. Impact of climate

478   and land cover change, J. Adv. Model. Earth. Sy., 10, 2829–2843.

479   https://doi.org/10.1029/2018MS001413, 2018.

480   Jia, B., Cai, X., Zhao, F., Liu, J., Chen, S., Luo, X., Xie, Z., and Xu, J.: Potential

481   future changes of terrestrial water storage based on climate projections by

482   ensemble model simulations, Adv. Water Resour., 142, 103635.

483   https://doi.org/10.1016/j.advwatres.2020.103635, 2020.

484   Jung, M., Reichstein, M., and Bondeau, A.: Towards global empirical upscaling of

485   FLUXNET eddy covariance observations: Validation of a model tree ensemble

486   approach using a biosphere model, Biogeosciences, 6, 2001–2013.

487   https://doi.org/10.5194/bg-6-2001-2009, 2009.

488   Kuang, X., and Jiao, J.: Review on climate change on the Tibetan Plateau during the

489   last half century, J. Geophys. Res. Atmos., 121, 3979‒4007.

490   https://doi.org/10.1002/2015JD024728, 2016.

491   Li, J., Liu, D., Li, Y., Wang, S., Yang, Y., Wang, X., Guo, H., Peng, S., Ding, J., Shen,

492   M., and Wang, L.: Grassland restoration reduces water yield in the headstream

493   region of Yangtze River, Sci. Rep., 7, 2162,

494   https://doi.org/10.1038/s41598-017-02413-9, 2017.

495   Li, W., Jiang, Z., Zhang, X., Li, L. and Sun, Y.: Additional risk in extreme

496   precipitation in China from 1.5 °C to 2.0 °C global warming levels, Sci.

497   Bull., 63, 228. https://doi.org/10.1016/j.scib.2017.12.021, 2018.

498   Liang, L., Li, L., Liu, C., and Cuo, L.: Climate change in the Tibetan Plateau Three

499   Rivers Source Region: 1960‒2009, Int. J. Climatol., 33, 2900-2916.

500   https://doi.org/10.1002/joc.3642, 2013.

501   Liang, X., Lettenmaier, D. P., Wood, E. F., and Burges, S. J.: A simple hydrologically

502   based model of land surface water and energy fluxes for general circulation

503 models, J. Geophys. Res., 99, 14,415-14,428. https://doi.org/10.1029/94JD00483,

504 1994.

505 Marcott, S. A., Shakun, J. D., Clark, P. U., and Mix, A. C.: A Reconstruction of

506 Regional and Global Temperature for the Past 11,300 Years, Science, 339, 1198

507 –1201. https://doi.org/10.1126/science.1228026, 2013.

508 Martens, B., Miralles, D. G., Lievens, H., van der Schalie, R., de Jeu, R. A. M.,

509 Fernández-Prieto, D., Beck, H. E., Dorigo, W. A., and Verhoest, N. E. C.:

510 GLEAM v3: satellite-based land evaporation and root-zone soil moisture, Geosci.

511 Model Dev., 10, 1903–1925. https://doi.org/10.5194/gmd-10-1903-2017, 2017.

512 Marx, A., Kumar, R., and Thober, S.: Climate change alters low flows in Europe

513 under global warming of 1.5, 2, and 3° C, Hydrol. Earth. Syst. Sc., 22, 1017–

514 1032. https://doi.org/10.5194/hess-22-1017-2018, 2018.

515 Meinshausen, M., Nicholls, Z. R. J., Lewis, J., Gidden, M. J., Vogel, E., Freund, M.,

516 Beyerle, U., Gessner, C., Nauels, A., Bauer, N., Canadell, J. G., Daniel, J. S.,

517 John, A., Krummel, P. B., Luderer, G., Meinshausen, N., Montzka, S. A., Rayner,

518 P. J., Reimann, S., Smith, S. J., van den Berg, M., Velders, G. J. M., Vollmer, M.

519 K., and Wang, R. H. J.: The shared socio-economic pathway (SSP) greenhouse

520 gas concentrations and their extensions to 2500, Geosci. Model Dev., 13, 3571–

521 3605, https://doi.org/10.5194/gmd-13-3571-2020, 2020.

522 Meinshausen, M., Vogel, E., and Nauels, A., Lorbacher, K., Meinshausen, N.,

523 Etheridge, D. M., Fraser, P. J., Montzka, S. A., Rayner, P. J., Trudinger, C. M.,

524 Krummel, P. B., Beyerle, U., Canadell, J. G., Daniel, J. S., Enting, I. G., Law, R.

525   M., Lunder, C. R., O'Doherty, S., Prinn, R. G., Reimann, S., Rubino, M., Velders,

526   G. J. M., Vollmer, M. K., Wang, R. H. J., and Weiss, R.: Historical greenhouse

527   gas concentrations for climate modelling (CMIP6), Geosci. Model Dev., 10,

528   2057-2116. https://doi.org/10.5194/gmd-10-2057-2017, 2017.

529   Mohammed, K., Islam, A. S., Islam, G. M. T., Alfieri, L., Bala, S. K., and Khan, M. J.

530   U.: Extreme flows and water availability of the Brahmaputra River under 1.5 and

531   2 ° C global warming scenarios, Climatic Change, 145, 159-175.

532   https://doi.org/10.1007/s10584-017-2073-2, 2017.

533   Morice, C. P., Kennedy J. J., Rayner N. A., and Jones P. D.: Quantifying uncertainties

534   in global and regional temperature change using an ensemble of observational

535   estimates: The HadCRUT4 dataset, J. Geophys. Res., 117, D08101.

536   https://doi.org/10.1029/2011JD017187, 2012.

537   Oleson, K. W., Lawrence, D. M., Bonan, G. B., Drewniak, B., Huang, M., Koven, C.

538   D., Levis, S., Li, F., Riley, W. J., Subin, Z. M., Swenson, S. C., Thornton, P. E.,

539   Bozbiyik, A., Fisher, R., Heald, C. L., Kluzek, E., Lamarque, J. F., Lawrence, P.

540   J., Leung, L. R., Lipscomb, W., Muszala, S., Ricciuto, D. M., Sacks, W., Sun, Y.,

541   Tang, J., Yang, Z. L.: Technical description of version 4.5 of the Community

542   Land Model (CLM) (Rep. NCAR/TN-503 + STR, 420), 2013.

543   O'Neill, B. C., Tebaldi, C., Vuuren, D. P. V., Eyring, V., Friedlingstein, P., Hurtt, G.,

544   Knutti, R., Kriegler, E., Lamarque, J. F., Lowe, J., Meehl, G. A., Moss, R., Riahi,

545   K., and Sanderson, B. M.: The scenario model intercomparison project

546   (ScenarioMIP) for CMIP6, Geosci. Model Dev., 9, 3461-3482.

547   https://doi.org/10.5194/gmd-9-3461-2016, 2016.

548 Samaniego, L., Kumar, R., Breuer, L., Chamorro, A., Flörke, M., Pechlivanidis, I. G.,

549   Schäfer, D., Shah, H., Vetter, T., Wortmann, M., and Zeng, X.: Propagation of

550   forcing and model uncertainties on to hydrological drought characteristics in a

551   multi-model century-long experiment in large river basins, Climatic Change, 141,

552   435-449. https://doi.org/10.1007/s10584-016-1778-y, 2017.

553 Thober, T., Kumar, R., and Waders, N.: Multi-model ensemble projections of

554   European river floods and high flows at 1.5, 2, and 3 degrees global warming,

555   Environ. Res. Lett., 13, 014003. https://doi.org/10.1088/1748-9326/aa9e35,

556   2018.

557 Vicente-Serrano, S. M., Lopez-Moreno, J. I., Begueria, S., Lorenzo-Lacruz, J.,

558   Azorin-Molina, C., and Moran-Tejeda, E.: Accurate computation of a streamflow

559   drought index, J. Hydrol. Eng., 17, 318 – 332.

560   https://doi.org/10.1061/(Asce)He.1943-5584.0000433, 2012.

561 Watkins, M. M., Wiese, D. N., Yuan, D. N., Boening, C., and Landerer, F. W.:

562   Improved methods for observing Earth's time variable mass distribution with

563   GRACE using spherical cap mascons, J. Geophys. Res. Solid Earth, 120,

564   2648-2671. https://doi.org/10.1002/2014JB011547, 2015.

565 Wiltshire, A., Gornall, J., Booth, B., Dennis, E., Falloon, P., Kay, G., McNeall, D.,

566   McSweeney, C. and Betts, R.: The importance of population, climate change and

567   CO_2 plant physiological forcing in determining future global water stress, Global

568   Environ.   Change,   23(5),   1083-1097.

569   http://dx.doi.org/10.1016/j.gloenvcha.2013.06.005, 2013.

570   WMO.: WMO Statement on the State of the Global Climate in 2019,

571   https://library.wmo.int/doc_num.php?explnum_id=10211, 2020.

572   Yang, K., Wu, H., Qin, J., Lin, C., Tang, W., and Chen, Y.: Recent climate changes

573   over the Tibetan plateau and their impacts on energy and water cycle: A review,

574   Global   Planet.   Change,   112,   79   –   91.

575   https://doi.org/10.1016/j.gloplacha.2013.12.001, 2013.

576   Yang, Y., Rodericj, M. L., Zhang, S., McVicar, T. R., and Donohue, R. J.: Hydrologic

577   implications of vegetation response to elevated CO2 in climate projections, Nat.

578   Clim. Change, 9, 44-48. https://doi.org/10.1038/s41558-018-0361-0, 2019.

579   Yuan, X., Ji, P., Wang, L., Liang, X., Yang, K., Ye, A., Su, Z., and Wen, J.: High

580   resolution land surface modeling of hydrological changes over the Sanjiangyuan

581   region in the eastern Tibetan Plateau: 1. Model development and evaluation, J.

582   Adv. Model. Earth. Sy., 10, 2806 – 2828. https://doi.org/10.1029/2018MS001413,

583   2018a.

584   Yuan, X., Jiao, Y., Yang, D., and Lei, H.: Reconciling the attribution of changes in

585   streamflow extremes from a hydroclimate perspective, Water Resour. Res., 54,

586   3886 – 3895. https://doi.org/10.1029/2018WR022714, 2018b.

587   Yuan, X., Zhang, M., Wang, L., and Zhou, T.: Understanding and seasonal forecasting

588   of hydrological drought in the Anthropocene, Hydrol. Earth. Syst. Sc., 21, 5477

589   – 5492. https://doi.org/10.5194/hess-21-5477-2017, 2017.

590   Zhang Y., You Q., Chen C., and Ge J.: Impacts of climate change on streamflows

591   under RCP scenarios: A case study in Xin River Basin, China, Atmos. Res.,

592   178-179, 521-534. http://dx.doi.org/10.1016/j.atmosres.2016.04.018, 2016.

593   Zhao Q., Ding Y., Wang J., Gao H., Zhang S., Zhao C. Xu J. Han H., and Shangguan

594   D.: Projecting climate change impacts on hydrological processes on the Tibetan

595   Plateau with model calibration against the glacier inventory data and observed

596   streamflow, J. Hydrol., 573, 60-81. https://doi.org/10.1016/j.jhydrol.2019.03.043,

597   2019.

598   Zhu Q., Jiang H., Peng C., Liu J,, Fang X., Wei X., Liu S., and Zhou G.: Effects of

599   future climate change, CO2 enrichment, and vegetation structure variation on

600   hydrological processes in China, Global Planet. Change, 80-81, 123-135.

601   https://doi.org/10.1016/j.gloplacha.2011.10.010, 2012.

602   Zhu, Z. C., Piao, S. L., Myneni, R. B., Huang, M. T., Zeng, Z. Z., Canadell, J. G.,

603   Ciais, P., Sitch, S., Friedlingstein, P., Arneth, A., Cao, C. X., Cheng, L., Kato, E.,

604   Koven, C., Li, Y., Lian, X., Liu, Y. W., Liu, R. G., Mao, J. F., Pan, Y. Z., Peng, S.

605   S., Penuelas, J., Poulter, B., Pugh, T. A. M., Stocker, B. D., Viovy, N., Wang, X.

606   H., Wang, Y. P., Xiao, Z. Q., Yang, H., Zaehle, S., and Zeng, N.: Greening of the

607   Earth   and   its   drivers,   Nature   Climate   Change,   6(8),   791-+,

608   https://doi.org/10.1038/Nclimate3004, 2016.

609

610
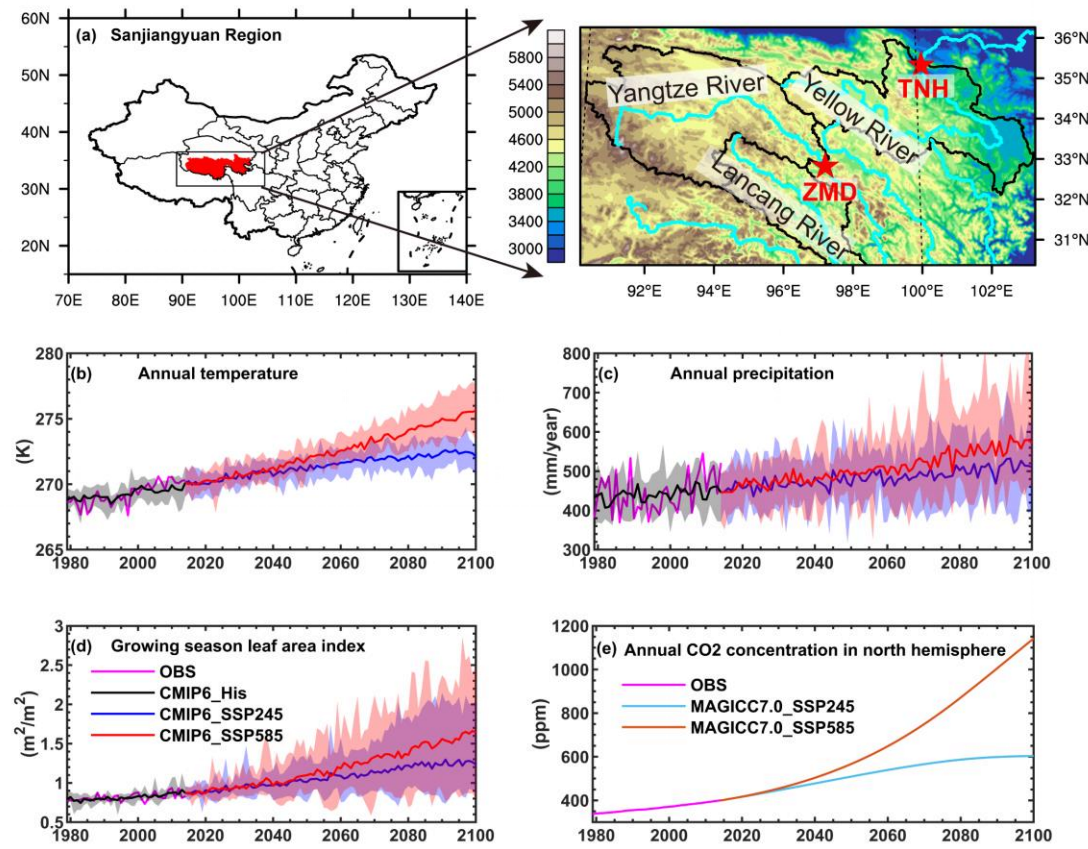
Figure 1. (a) The locations of the Sanjiangyuan region and streamflow gauges. (b)-(e)

are the time series of annual temperature, precipitation, growing season leaf area

index and CO_2 concentration averaged over the Sanjiangyuan region during

1979-2100. Red pentagrams in (a) are two streamflow stations named Tangnaihai

(TNH) and Zhimenda (ZMD). Black, blue and red lines in (b-d) are ensemble means

of CMIP6 model simulations from the historical, SSP245 and SSP585 experiments.

Shadings are ranges of individual ensemble members. Cyan and brown lines in (e) are

future CO_2 concentration under SSP245 and SSP585 scenarios simulated by

MAGICC7.0 model.

620

621
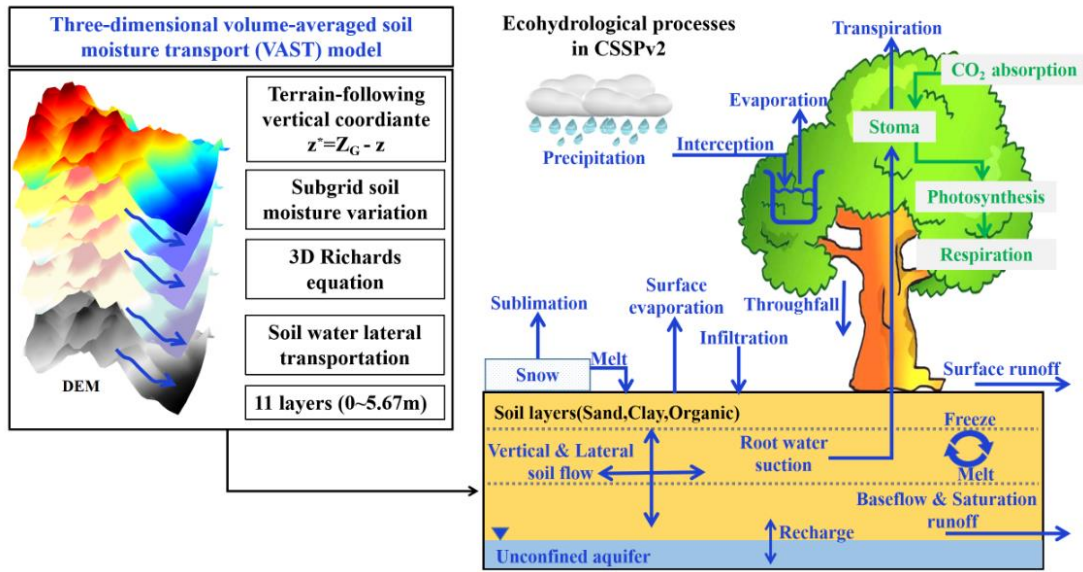
622

623 **Figure 2.** Structure and main ecohydrological processes in the Conjunctive

624 Surface-Subsurface Process version 2 (CSSPv2) land surface model.
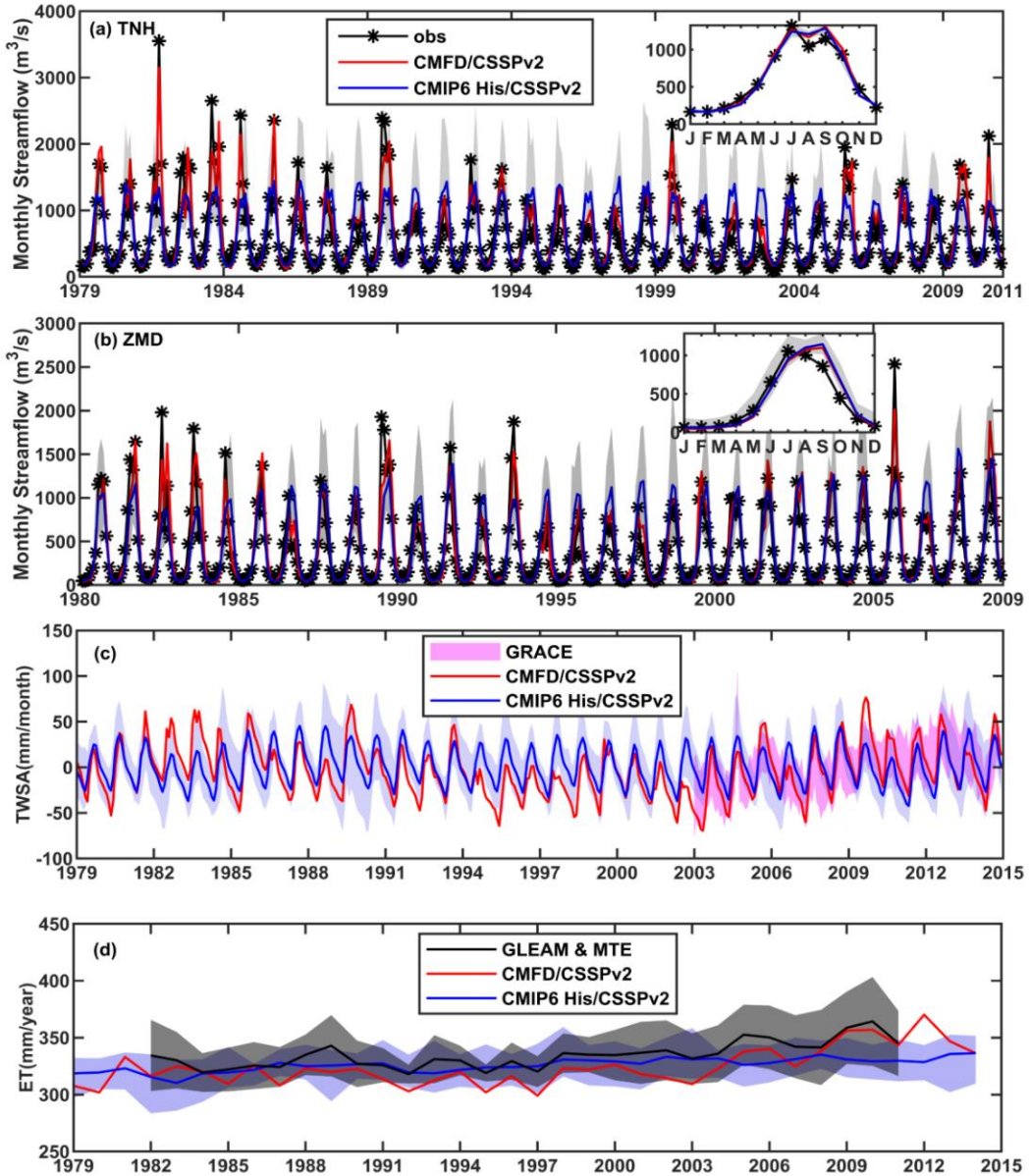
Figure 3. Evaluation of model simulations. (a-b) Observed and simulated monthly

streamflow at the Tangnaihai (TNH) and Zhimenda (ZMD) hydrological stations, with

the climatology shown in the upper-right corner. (c-d) Evaluation of the simulated

monthly terrestrial water storage anomaly (TWSA) and annual evapotranspiration (ET)

averaged over the Sanjiangyuan region. Red lines are CSSPv2 simulation forced by

observed meteorological forcing. Blue lines represent ensemble means of 11

CMIP6_His/CSSPv2 simulations, while gray shadings in (a-b) and blue shadings in

(c-d) are ranges of individual ensemble members. Pink shading in (c) is GRACE

634   satellite observations. Black line and black shading in (d) are ensemble mean and

635   ranges of GLEAM_ET and MTE_ET datasets.

636

637

638
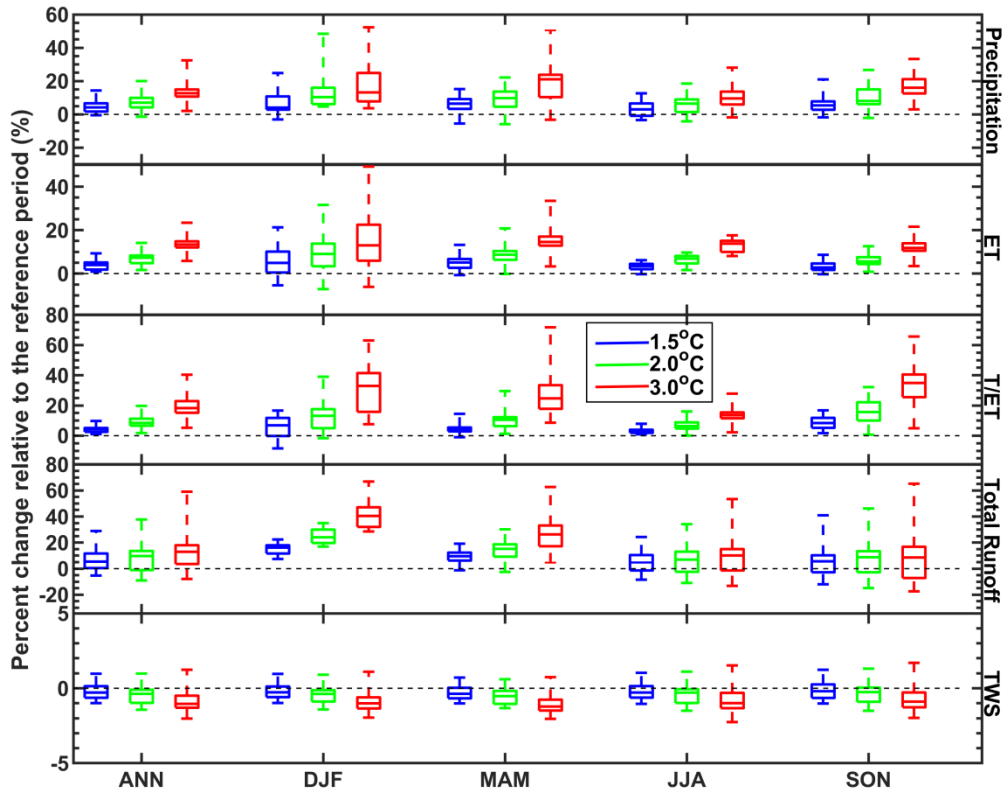
Figure 4. Box plots of relative changes of regional mean precipitation, evapotranspiration (ET), ratio of transpiration to evapotranspiration (T/ET), total runoff and terrestrial water storage (TWS) at different global warming levels. Reference period is 1985-2014, and annual (ANN) and seasonal (winter: DF, spring: MAM, summer: JJA and autumn: SON) results are all shown. Boxes show 25th to 75th ranges among 22 CMIP6_SSP/CSSPv2 simulations, while lines in the boxes are median values.

646

647
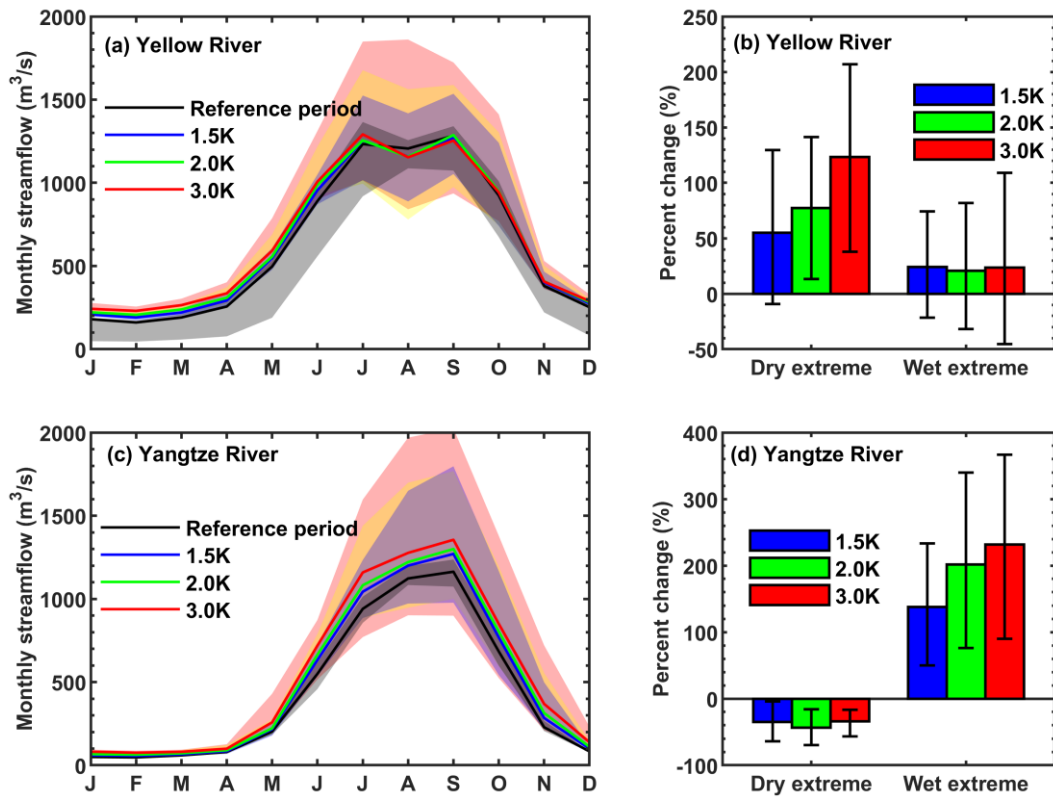
Figure 5. Changes of streamflow and its extremes at the outlets of the headwater

regions of the Yellow river and the Yangtze river, i.e., Tangnaihai gauge and

Zhimenda gauge. (a) Simulated monthly streamflow over the Yellow river during the

reference period (1985-2014) and the periods with different global warming levels.

Solid lines represent ensemble means, while shadings are ranges of individual

ensemble members. (b) Percent changes in frequency of dry and wet extremes in

July-September at different warming levels. Colored bars are ensemble means, while

error bars are 5~95% uncertainty ranges estimated by using bootstrapping for 10,000

times. (c) and (d) are the same as (a) and (b), but for the Yangtze river.

657

658
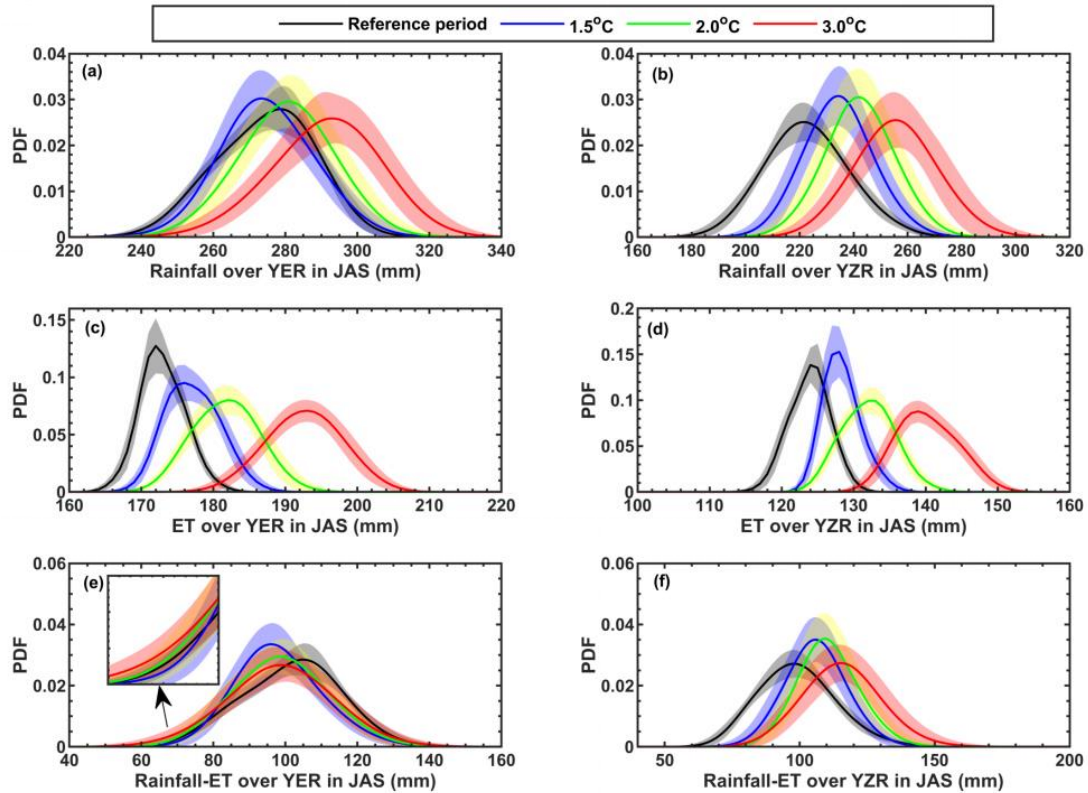
Figure 6. Probability density functions (PDFs) of regional mean rainfall, evapotranspiration (ET) and their difference over the headwater regions of Yellow river (YER) and Yangtze river (YZR) during flooding seasons (July-September) for the reference period (1985-2014) and the periods with 1.5, 2.0 and 3.0 ℃ global warming levels. Shadings are 5~95% uncertainty ranges.

664

665
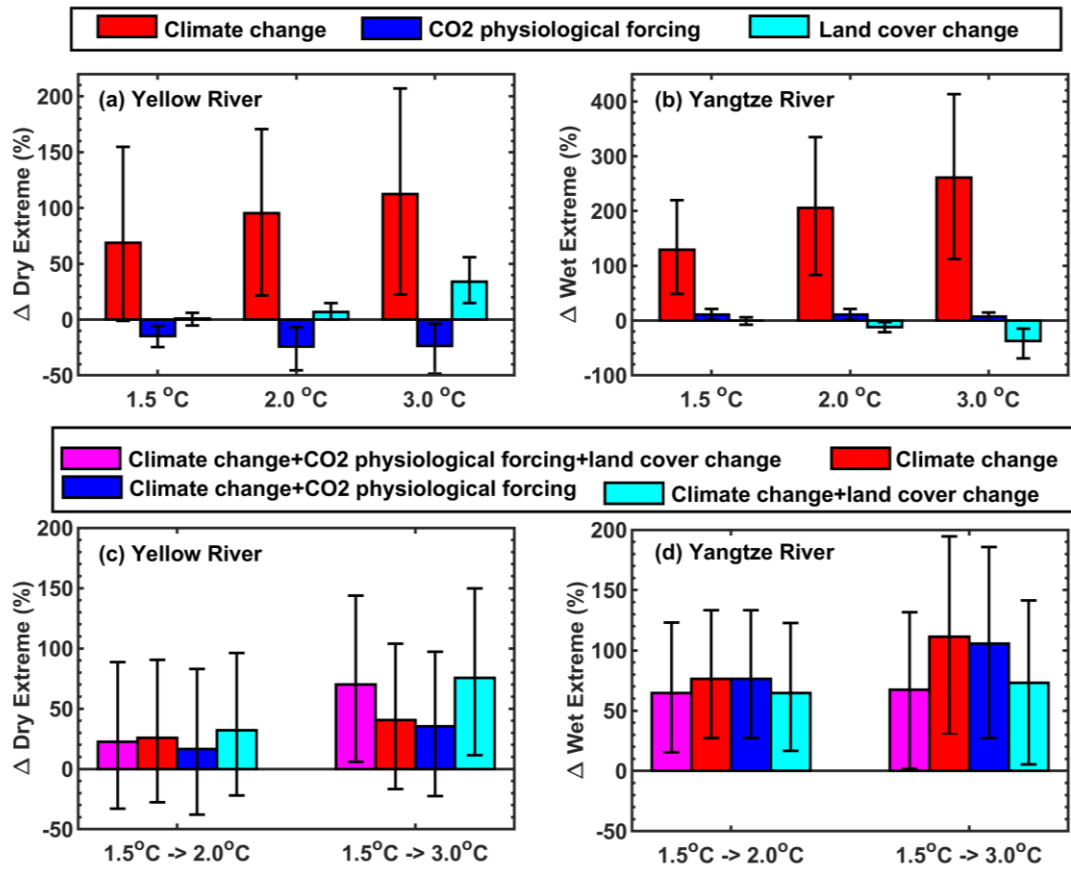
Figure 7. (a-b) Influences of climate change, CO_2 physiological forcing and land

cover change on relative changes in frequency of the dry and wet extremes in

July-September at different global warming levels for the headwater regions of

Yellow river and Yangtze river. (c-d) Changes of dry and wet extremes under

additional warming of 0.5 ℃ and 1.5 ℃ with the consideration of different factors. All

the changes are relative to the reference period (1985-2014). Ensemble means are

shown by colored bars while the 5~95% uncertainty ranges estimated by using

bootstrapping for 10,000 times are represented by error bars.

674

675 **Table 1.** CMIP6 simulations used in this study. His means historical simulations

676 during 1979-2014 with both anthropogenic and natural forcings, SSP245 and SSP585

677 represent two Shared Socioeconomic Pathways during 2015-2100. Note the

678 CNRM-CM6-1 and CNRM-ESM2-1 do not provide r1i1p1f1 realization, so r1i1p1f2

679 was used instead.

No.	Models	Experiments	Realization	Horizontal Resolution (Longitude $\times$ Latitude Grid Points)
1	ACCESS-ESM1-5	His/SSP245/SSP585	r1i1p1f1	192×145
2	BCC-CSM2-MR	His/SSP245/SSP585	r1i1p1f1	320×160
3	CESM2	His/SSP245/SSP585	r1i1p1f1	288×192
4	CNRM-CM6-1	His/SSP245/SSP585	r1i1p1f2	256×128
5	CNRM-ESM2-1	His/SSP245/SSP585	r1i1p1f2	256×128
6	EC-Earth3-Veg	His/SSP245/SSP585	r1i1p1f1	512×256
7	FGOALS-g3	His/SSP245/SSP585	r1i1p1f1	180×80
8	GFDL-CM4	His/SSP245/SSP585	r1i1p1f1	288×180
9	INM-CM5-0	His/SSP245/SSP585	r1i1p1f1	180×120
10	MPI-ESM1-2-HR	His/SSP245/SSP585	r1i1p1f1	384×192
11	MRI-ESM2-0	His/SSP245/SSP585	r1i1p1f1	320×160

680

681 **Table 2.** Determination of "crossing years" for the periods reaching 1.5, 2 and 3 ℃

682 warming levels for different GCM and SSP combinations.

Models	1.5 ℃ warming level		2.0 ℃ warming level		3.0 ℃ warming level	
	SSP245	SSP585	SSP245	SSP585	SSP245	SSP585
ACCESS-ESM1-5	2024	2023	2037	2034	2070	2052
BCC-CSM2-MR	2026	2023	2043	2034	Not found	2054
CESM2	2024	2022	2037	2032	2069	2048
CNRM-CM6-1	2032	2028	2047	2039	2075	2055
CNRM-ESM2-1	2030	2026	2049	2039	2075	2058
EC-Earth3-Veg	2028	2023	2044	2035	2072	2053
FGOALS-g3	2033	2032	2063	2046	Not found	2069
GFDL-CM4	2025	2024	2038	2036	2073	2053
INM-CM5-0	2031	2027	2059	2038	Not found	2063
MPI-ESM1-2-HR	2032	2030	2055	2044	Not found	2066
MRI-ESM2-0	2024	2021	2038	2030	2074	2051

683

684 Table 3. Performance for CSSPv2 model simulations driven by the observed

685 meteorological forcing (CMFD/CSSPv2) and the bias-corrected CMIP6 historical

686 simulations (CMIP6_His/CSSPv2). The metrics include correlation coefficient (CC),

687 root mean squared error (RMSE), and Kling-Gupta efficiency (KGE).

Variables	Experiments	CC	RMSE	KGE
Monthly streamflow over TNH	CMFD/CSSPv2	0.95	165 m^3/s	0.94
	CMIP6_His/CSSPv2	0.76	342 m^3/s	0.71
Monthly streamflow over ZMD	CMFD/CSSPv2	0.93	169 m^3/s	0.91
	CMIP6_His/CSSPv2	0.82	257 m^3/s	0.81
Monthly terrestrial water storage anomaly over the Sanjiangyuan region	CMFD/CSSPv2	0.7	22 mm/month	-
	CMIP6_His/CSSPv2	0.4	24 mm/month	-
Annual evapotranspiration over the Sanjiangyuan region	CMFD/CSSPv2	0.87	14 mm/year	-
	CMIP6_His/CSSPv2	0.47	13 mm/year	-

688

689